De nition of a adaptation methodology of the models of assistance and experimental validation.

Valentina Ciarla, Carlos Canudas de Wit, Jonathan Dumon, Franck Quaine, Violaine Cahouet

Definition of a adaptation methodology of the models of assistance and experimental validation.

V. Ciarla, C. Canudas de Wit, J. Dumon, F. Quaine, V. Cahouet

GIPSA-Lab, UMR 5216, France

Abstract

This document is a preliminary version of the working report concerning the work packages 5.3 and 5.4 of the project **VolHand 09 VTT 14**, that are in charge to the Gipsa-Lab.
In this working report, authors introduce the general architecture used to simulate the Electronic Power Steering (EPS) system for a standard and a non-standard driver. In this first part, the models, the controller and the observer used for the simulation are introduced. Then, the methodology used to adapt the model to a non-standard driver is described in detail. Finally, the experimental validation of this general architecture is proposed.
Section 2 refers to the module Gipsa-Comp. Section 3 concerns the module Gipsa-Obs. Section 4 is dedicated to the module Gipsa-Booster. The module Gipsa-Tune is under development.

1 INTRODUCTION

In order to study the general methodology for the adaptation of the classical amplification curves to disabled people, an interview has been done to a sample of manufacturers that adapt the vehicles to the patient. The following points emerged from these investigations:

- The adaptation of the vehicle is decided by the *Prefecture*, when releases the driving license to the patient. This organ decides what is the adaptation mechanism that the patient needs (for example, the ball on the steering wheel for drivers with one hand).
- In case of disabilities to the upper limbs, the following mechanisms are used:
  - **Removable ball** on the steering wheel, in case of total/partial invalidity to one of the two arms. About the position of the ball on the steering wheel, there is not a clear policy, because some manufacturers (such as Hand-drive) mount the ball at the top/center of the steering wheel. Some others (such as Hand-mobile or Ceremh) mount the ball on the side of the healthy arm. In particular, they consider the steering wheel as a clock and they mount the ball at 2 PM for the right hand and at 10 AM for the left hand.
    A radio command can be mounted close to the ball to allow the driver to activate headlights/flashes and show the position. In some cases, a lever is mounted on the opposite side to brake/accelerate the vehicle. This lever is directly linked to the brake/acceleration pedals. This is the case of patients without problems of prehension (gripping ability) or quadriplegic. This last case is not clear, because some manufacturers (Hand-drive) prefer to use a double steering wheel mounted upper (or over) the normal steering wheel, instead of the ball and the lever.

(a) (b)

Figure 1: Examples of (a) ball mounted on the steering wheel for total/partial invalidity; (b) radio command used to show the visibility of the vehicle.

  - **Forks** on the steering wheel, in case of a good mobility of the wrist, but bad mobility of the fingers.
  - **Tripod**, in case of partial/complete invalidity of the wrist and the fingers.

All these adaptation mechanisms are compatible with the standard assistance systems (ABS, EPS, etc..), that is possible to find on a commercial vehicle. Starting from these considerations, it is possible to divide the drivers in two large clusters:

1. standard drivers, who have the correct functionality of the upper limb;
2. non-standard drivers, who are obliged to drive with only one hand, with the use of one of the previous mechanism described above.

The adaptation methodology has been developed starting from a control framework, designed for a standard driver, and has been extended to non-standard drivers with the introduction of additional blocks. This document has the goal to introduce the results of the work packages 5.3 and 5.4. In particular, the first aim is to validate the theoretical results concerning the oscillation annealing control

(a)

(b)

Figure 2: Examples of (a) forks in case of good mobility of the wrist, but bad mobility of the fingers; (b) tripod in case of partial/complete invalidity of the wrist and the fingers.

and the observer using a HIL setup and to verify the compatibility of these elements with the classical booster stage (part of the task 5.4). In this section, an additional validation is done, concerning the tire-road friction model. A comparison between the simulated friction torque and the real one is done, in order to show that the model prediction is realistic. The second part concerns the analysis of the methodology to adapt the general architecture for non-standard drivers. An experimental validation is also proposed at the end of this part (task 5.4).

1.1 General architecture of the EPAS system

The general architecture, that is proposed for the driver's profiles, is shown in Fig. 3 and can be described as follows:

1. The **model of the vehicle**, that includes both the model of the steering wheel column and the bicycle model to obtain informations about the lateral dynamics of vehicle.
   The exogenous inputs acting on the vehicle are the **driver's exerted torque** and the **tire-road friction** torque. Both these sub-systems are modelled in order to obtain a realistic behaviour. The driver is modelled as a position tracking control. The friction model is used to describe the Sticking and the Self-Alignment phenomena. The first one appears at lows speed of the vehicle, in opposition to the movement of the wheels during parking manoeuvre. The second one brings the wheels at their vertical axes during high speed driving.

2. In open loop, the steering system is affected by undesired oscillations that can be compensated with an optimal **inner control loop**. From the available measures of this system, it is possible to design an **observer** to estimate the exogenous inputs acting on it.

3. **Booster stage**: it provides the necessary amplification torque during the driving. It takes in input the driver's exerted torque and the vehicle speed and provides in output the assistance torque, necessary to improve the driving comfort. The behaviour differs according to the driver: for a standard driver, the classical amplification curves are employed. For non-standard drivers,

the standard parameters change to let the booster curve to provide a more adapted assistance. Moreover, a **tuning mechanism** is employed to provide additional informations to the booster stage. Note that the adaptation can be implemented via software, without modifications to the hardware of the system.

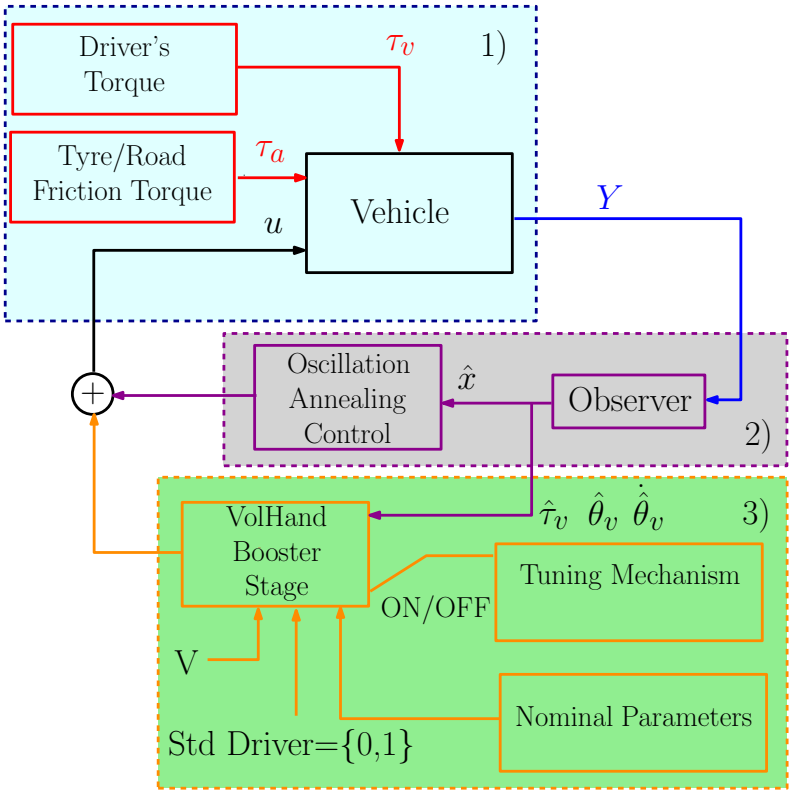

Figure 3: Model of the general architecture of the EPAS system

2 MODELS FOR SIMULATIONS

This section is dedicated to the description of the mathematical models used to simulate the general architecture for the EPAS system. First, the mechanical model of the steering column and the electrical motor is introduced; then, the description of the tire-road friction torque and of the driver's model is done. This model takes in input the measure of the slip angle of the vehicle, so an introduction to the simple bicycle model used to obtain this measure is done.

2.1 Model of the EPS system

The mathematical model of the EPS that authors take into account is based on works in [5], [9] and [6]. The model is shown in Fig. 4 and can be described by the following set of linear differential equations:

$$J_v\ddot{\theta}_v = \tau_v - k(\theta_v - \theta_s) - B_v\dot{\theta}_v \quad (1)$$

$$J_T\ddot{\theta}_s = -k(\theta_s - \theta_v) - N_2^2 B_m\dot{\theta}_s + \frac{\tau_a}{N_1} + N_2 u \quad (2)$$

with $J_T = \left(J_c + N_2^2 J_m + \frac{J_w}{N_1^2}\right)$ is the total inertia at the column, motor and rack. The constants of the model are defined in Table 1, while θ_v, θ_s and θ_m correspond to the angular positions of the steering wheel, the steering column and the motor. Let introduce the following state-space variables:

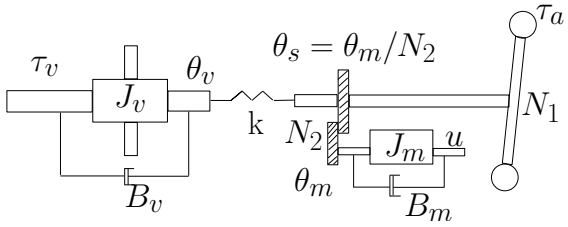

Figure 4: Mechanical model of the EPS system

$$x^T = \left(x_1, x_2, x_3\right)^T = \left(\dot{\theta}_v, \dot{\theta}_s, \theta_v - \theta_s\right)^T \quad (3)$$

The model can be formulated into the state-space form $\dot{x} = Ax + Bu + Gw$ with the exogenous inputs $w = \left(\tau_v, \tau_a\right)^T$ and the state-space matrices

$$A = \begin{pmatrix} -\frac{B_v}{J_v} & 0 & -\frac{k}{J_v} \\ 0 & -\frac{N_2^2 B_m}{J_T} & \frac{k}{J_T} \\ 1 & -1 & 0 \end{pmatrix}; \quad B = \begin{pmatrix} 0 \\ \frac{N_2}{J_T} \\ 0 \end{pmatrix};$$

$$G = \begin{pmatrix} \frac{1}{J_v} & 0 \\ 0 & \frac{1}{N_1 J_T} \\ 0 & 0 \end{pmatrix} = \begin{bmatrix} g_1 & g_2 \end{bmatrix}; \quad (4)$$

The control input u is actuated from the electrical motor at the basis of the steering column. It has two goals: to anneal the oscillations of the steering column and to amplify the driver's exerted torque, in order to guarantee a better driving feeling.

2.2 Linear bicycle model

The model under consideration is well known in literature ([1], [17], [3]) and is based on the following assumptions:

- Linear lateral tire friction curve, i.e.:

$$\begin{cases} F_{tyf} = C_{yf}\beta_f \\ F_{tyr} = C_{yr}\beta_r \end{cases} \quad (5)$$

  where C_{yf} and C_{yr} are the linear stiffness of the lateral tire characteristics at the front and rear, respectively.

Symbol	Description	Value
J_v	Steering wheel inertia	0.05 kgm^2
J_m	Motor inertia	0.0004 kgm^2
J_c	Column inertia	0.04 kgm^2
J_w	Rack inertia	0.000784 kgm^2
k	Column stiffness	100 $\mathrm{N\,m\,rad}^{-1}$
N_1	Steering column-wheels gear ratio	13.67
N_2	Motor-steering column gear ratio	17
B_v	Steering wheel viscosity	0.06 $\mathrm{N\,m\,rad}^{-1}\,\mathrm{s}^{-1}$
B_m	Motor shaft viscosity	0.0032 $\mathrm{N\,m\,rad}^{-1}\,\mathrm{s}^{-1}$
J_0	Wheel real inertia of the HIL setup	0.0303 kgm^2
B_0	Wheel real viscosity of the HIL setup	0.039 $\mathrm{N\,m\,rad}^{-1}\,\mathrm{s}^{-1}$
m	Vehicle total mass	1621 kg
l_f	Distance from the center of gravity to the front axle	1.15 m
l_r	Distance from the center of gravity to the rear axle	1.38 m
I_z	Vehicle inertia	1975 kgm^2
C_{yf}	Front axle tire cornering	28559 $\mathrm{N\,rad}^{-1}$
C_{yr}	Rear axle tire cornering	40698 $\mathrm{N\,rad}^{-1}$

Table 1: Parameters of the EPS system and the bicycle model

- Small slip angles (β_f and β_r):

$$\begin{cases} \beta_f = \theta_v - \beta - \frac{l_f \dot{\psi}}{v} \\ \beta_r = \beta + \frac{l_r \dot{\psi}}{v} \end{cases} \tag{6}$$

  where $\dot{\psi}$ denotes the vehicle yaw rate, β_f and β_r denote the slip angles at the front and rear, while θ_v is the steering angle of the front wheel.

Under these assumptions, the linearized model is given by (where v is a model parameter):

$$\begin{bmatrix} \ddot{\psi} \\ \dot{\beta} \end{bmatrix} = \begin{bmatrix} -\frac{l_f^2 C_{yf} + l_r^2 C_{yr}}{I_z v} & \frac{l_r C_{yr} - l_f C_{yf}}{I_z} \\ -1 + \frac{l_r C_{yr} - l_f C_{yf}}{m v^2} & -\frac{(C_{yf} + C_{yr})}{mv} \end{bmatrix} \begin{bmatrix} \dot{\psi} \\ \beta \end{bmatrix} + \begin{bmatrix} \frac{l_f C_{yf}}{I_z} \\ \frac{C_{yf}}{mv} \end{bmatrix} \theta_v \tag{7}$$

Note that this model is not defined for speeds of the vehicle that are null. This is not a problem, because the Self-Alignment torque appears at high speeds. The values of the parameters are given in Table 1.

2.3 Dynamic tire-road friction model

The friction model used in this paper refers to the dynamic LuGre friction model, developed in [20], [7] and [11]. Most important components captured from this model are:

- Sticking torque M_{stick}, that opposes to the movement of the tyres when turning them around the vertical axis at low speeds of the vehicle.
- Self-Alignment $M_{self-align}$ torque, that appears at highs speeds and tends to rotate the wheels around their vertical axis, letting them to return to their vertical position.

Both these models derive from models at distributed parameters, where the friction force depends from the deflections $z_i(t, \zeta)$ of the patch element along x and y directions respectively, located at the point ζ with respect to the patch frame at a certain time t [20]. Nevertheless, the distributed models may not be easy to use for analysis and control design. For this reason, the corresponding lumped models are introduced.

2.3.1 Model of the Sticking torque

The internal state of the model is obtained from the differential equation

$$\dot{z}_z = \dot{\phi} - \frac{\sigma_{0z} |\dot{\phi}|}{g_z(\dot{\phi})} z_z \tag{8}$$

with the angular velocity of the wheel rim is $\dot{\phi} = \dot{\theta}_s / N_1$. The function

$$g_z\left(\dot{\phi}\right) = \mu_{kz} + \left(\mu_{sz} - \mu_{kz}\right) e^{-\left(\frac{\dot{\phi}}{\dot{\phi}_s}\right)^2} \tag{9}$$

determines the steady-state behaviour of the model. The parameters μ_{kz} and μ_{sz} are, respectively, the kinetic and static friction coefficients across the z-axis, while $\dot{\phi}_s$ is the Stribeck velocity. The corresponding torque is given by

$$M_{sticking} = -LF_n(\sigma_{0z} z_z + \sigma_{1z}\dot{z}_z + \sigma_{2z}\dot{\phi})e^{-|v|/v_k} \tag{10}$$

The dependency from the cruise speed of the vehicle v allows to simulate the effect that at high speeds the sticking toque is almost negligible, if compared to the self-alignment torque.

2.3.2 Model of the Self-Alignment torque

Let $\bar{z}_i$ $(i = x, y)$ and $\hat{z}_y$ denote the internal states of the system:

$$\dot{\bar{z}}_i = v_{ri} - C_{0i}(v_r)\bar{z}_i - \kappa_i^{ss}|\omega r|\bar{z}_i(t) \text{ for (i = x, y)} \tag{11}$$

$$\dot{\hat{z}}_y = \frac{G}{F_n L} v_{ry} - C_{0y}(v_r)\hat{z}_y - \nu^{ss}|\omega r|\hat{z}_y + \frac{|\omega r|}{L}\bar{z}_y \tag{12}$$

In Eqs. (11) and (12), it is possible to recognize the vector of the relative speeds v_{ri} $(i = x, y)$:

$$v_r = \begin{bmatrix} v_{rx} \\ v_{ry} \end{bmatrix} = \begin{bmatrix} \omega r - v cos(\beta) \\ -v sin(\beta) \end{bmatrix} \tag{13}$$

This vector depends on the angular velocity ω of the wheel, the radius r and the slip angle β.
The scalar function $C_{0i}(v_r)$ (with i = x, y) is given by:

$$C_{0i}(v_r) = \frac{||M_k^2 v_r||\sigma_{0i}}{g(v_r)\mu_{ki}^2} \tag{14}$$

with

$$g\left(v_r\right) = \frac{\left\|M_k^2 v_r\right\|}{\|M_k v_r\|} + \left(\frac{\left\|M_s^2 v_r\right\|}{\|M_s v_r\|} - \frac{\left\|M_k^2 v_r\right\|}{\|M_k v_r\|}\right) e^{-\left(\frac{\|v_r\|}{v_s}\right)^\gamma} \tag{15}$$

It depends on the diagonal matrices M_k and M_s of the kinetic and static friction coefficients

$$M_k = \begin{bmatrix} \mu_{kx} & 0 \\ 0 & \mu_{ky} \end{bmatrix} > 0 \tag{16}$$

$$M_s = \begin{bmatrix} \mu_{sx} & 0 \\ 0 & \mu_{sy} \end{bmatrix} > 0 \tag{17}$$

The constants κ_i^{ss} and ν^{ss} in Eqs. (11) and (12) can be obtained from the hypothesis that the steady-state solution of the lumped model is the same as the steady-state solution of the distributed one. The complete expression of these parameters is given from:

$$\kappa_i^{ss} = \frac{1}{|\omega r|}\left(\frac{v_{ri}}{\bar{z}_i^{ss}} - C_{0i}(v_r)\right) \tag{18}$$

$$\nu^{ss} = \frac{1}{|\omega r|}\left(\frac{1}{\hat{z}_y^{ss}}\left(\frac{G v_{ry}}{F_n L} + \frac{|\omega r|\bar{z}_y^{ss}}{L}\right) - C_{0y}\right) \tag{19}$$

with $\bar{z}_i^{ss}$ and $\hat{z}_y^{ss}$, that are the steady-states of the system. The explicit expression for these parameters is given in the appendix of [20]. The self-alignment torque can be written in terms of the mean states $\bar{z}_y$ and $\hat{z}_y$ as follows:

$$\begin{aligned} M_{self-alig} = F_n L\Big[&\sigma_{0y}\left(\frac{1}{2}\bar{z}_y(t) - \hat{z}_y\right) \\ &+ \sigma_{1y}\left(\frac{1}{2}\dot{\bar{z}}_y - \dot{\hat{z}}_y\right) + \sigma_{2y}\left(\frac{1}{2}v_{ry} - \frac{G}{F_n L}\right)\Big] \end{aligned} \tag{20}$$

The parameters used in this model are reported in Table 2. Hence, the total torque generated by the contact between the tires and the road is:

$$\tau_a = M_{stick} + M_{self-alig} \tag{21}$$

The validation of this model was proposed in [11], where authors show that the proposed models respect the expected behaviour: at low speeds the sticking torque M_{stick} is more important than the self-alignment torque $M_{self-alig}$; at higher speeds of the vehicle, the self-alignment torque is higher and turns the wheels to their vertical position.

Symbol	Value	Description
r	wheel radius	0.4 m
σ_{0z}	normalized rubber stiffness z-axis	20 m^{-1}
σ_{1z}	normalized rubber damping z-axis	0.0023 $\mathrm{s\,m}^{-1}$
σ_{2z}	normalized viscous relative damping z-axis	0.0001 $\mathrm{s\,m}^{-1}$
$\dot{\phi}_s$	Stribeck relative angular velocity	74 $\mathrm{rad\,s}^{-1}$
μ_{kx}	coeff. of kinetic friction x-axis	0.75
μ_{ky}	coeff. of kinetic friction y-axis	0.75
μ_{kz}	coeff. of kinetic friction z-axis	0.76
μ_{sx}	coeff. of static friction x-axis	1.35
μ_{sy}	coeff. of static friction y-axis	1.40
μ_{sz}	coeff. of static friction z-axis	0.91
v_s	Stribeck relative velocity	3.96 $\mathrm{m\,s}^{-1}$
γ	steady state constant	1
σ_{0y}	normalized rubber stiffness y-axis	470 m^{-1}
σ_{1y}	normalized rubber damping y-axis	0.327 $\mathrm{s\,m}^{-1}$
σ_{2y}	normalized viscous relative damping y-axis	0 $\mathrm{s\,m}^{-1}$
L	patch length	0.3 m
ζ_L	left patch length	0.0030 m
ζ_R	right patch length	0.1155 m
F_{max}	max normal force	1900 N
F_n	normal force	249.37 N
G	constant of the load distribution	16.83 Nm^2
κ_i^{ss}	constant of the lumped model	11.9
ν^{ss}	constant of the lumped model	-0.8

Table 2: Constant parameters of the LuGre model

2.4 Model of the driver

A standard driver, that is not affected by any pathology to the upper limbs, represents a closed kinematic chain with the steering wheel. He is symmetric around his upper limb and can choose to use the best placed arm to turn the wheel. In literature, he is considered as a feedback controller that takes into account of the path previewed information [14, 10]. The control takes in input the reference trajectory θ_{ref} and the steering wheel position θ_v and calculates the tracking error at each time instant t:

$$e = \theta_{ref} - \theta_v \tag{22}$$

The output of the controller corresponds to the driver's brain response and it is multiplied by the physical action time delay T. This element can be identified as the muscular torque τ_m and depends on the cognitive ability of the driver. As the main goal of this report is not the precise modeling of a standard driver's behavior, a simple Proportional Integrative Derivative (PID) control with a time delay is used to model it. In addition of the muscular torque τ_m, the weight of each arm produces a torque on the wheel. This element can be assumed as a disturb input, depending on the steering wheel position θ_v and others constant terms, that project the weight force on the plane of the steering wheel. Let define this disturb $\tau_w(\theta_v)$, as follows:

$$\tau_w(\theta_v) = mgR\cos(\phi)\sin(\theta_v - \theta_0) \tag{23}$$

where ϕ defines the inclination of the steering wheel with respect to the z axis and θ_0 corresponds to the position of the arm on the wheel. Under these considerations, the total driver's exerted torque can be defined as the sum:

$$\tau_v = \tau_m + \tau_w(\theta_v) \tag{24}$$

Note that the only unknown parameter is the mass of the arm[1]. It can be obtained throughout the use of anthropometric tables [21] or with an off-line estimation procedure.
For the sake of simplicity, we choose to restrict the domain of the study to patients who can drive with only one hand, because of total or partial invalidity to the other one. The European directive 2007/46/CE imposes that the adaptation of the steering wheel for these patients consists into the use of a ball, mounted at the upper centrer of the steering wheel or at $\pm 60°$ on the side of the healthy arm. If we make the comparison with the model of a standard driver, it is possible to make the hypothesis that the cognitive ability is the same, meaning that both behave as feedback controller. The difference is the ability to act halved. Moreover, the arm having an aymmetric capacity to act, the standard driver can choose at every moment arm best suited to apply a given torque to the steering wheel. In the case of conducting with one arm, some tasks are more difficult to accomplish than others.

3 CONTROL AND OBSERVER DESIGN

This section is dedicated to recall the design of a state-feedback control and of an exogenous input observer for the EPS system, shown in [11]. For sake of simplicity, in this paper the details concerning the control/observer synthesis are not reported. Nevertheless, these elements are part of the general architecture proposed for a standard driver profile and can be used also for a non-standard driver. In particular, the state control contribute to anneal the low frequency oscillations of the steering column. The estimation of the driver's exerted torque is used as input for the driver's assistance blocks, described in Section 4.

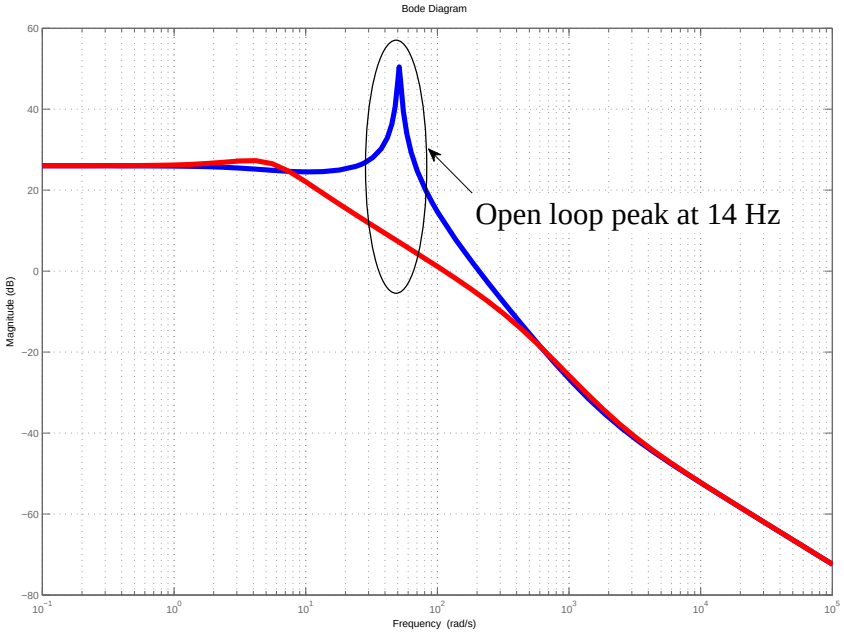

Figure 5: Bode diagram of the system in open loop (blue) and in closed loop.

3.1 State feedback control and torque observer

In [11], authors show that EPS system becomes unstable when there is a variation of the driver's exerted torque τ_v. The instability is physically due to the torsion of the steering column and it is possible to verify it looking at the frequency response of the system. To compensate these oscillations, an optimal LQR controller is designed. The resonance peak that might cause undesirable oscillations has been eliminated thanks to the proposed optimal linear control, as shown in Fig. 5. Note also that the low-frequency gain has kept unchanged. Details concerning the synthesis of this controller are shown in [11].

[1] To estimate the torque exerted by the mass of the healthy arm of the driver, an off-line estimation procedure is adopted. The theory about this procedure is under study and concerns the module Gipsa-Tuning

In [11], authors designed a full state observer for the exogenous inputs estimation, for instance the driver's exerted torque and the tire-road load friction torque. The observer was designed under the hypothesis of a slow-time variation of the exogenous inputs $\dot{\tau}_v \approx \dot{\tau}_v = 0$, that have been added as state variables to the original EPS system in Eq. (4). The measures of the column-shaft rate $\dot{\theta}_s$ and the column torsion $F_t = k(\theta_v - \theta_s)$ are taken into account to guarantee the observability of the system. In this paper, the estimation of the driver's torque $\hat{\tau}_v$ is used as input for the assistance system shown in Section 4, instead of the torsion measure, that is commonly used in automotive. The advantage is that the estimated measure is not affected by mechanical noise and its precision is not limited to the inertia and the viscosity of the steering column, as it happens when the column torsion is considered.

4 DRIVER'S ASSISTANCE SYSTEM

Main goal of the adaptation methodology is to generalize the standard assistance to the case of patients with a partial or total disability to the upper limb.
The common way to provide the steering assistance is throughout the use of static booster curves, that correspond to working points of the electrical motor ([22], [8],[13], [18], [2], [12])). For a given value of speed of the vehicle V and of the driver's exerted torque τ_v, the electrical motor provide in output the corresponding assistance torque u_{ass}. Indeed, these curves do not provide the same steering feel as the widely diffused hydraulic technology. The reason is that the hydraulic cycle is characterized by an hysteresis curve, that is not reproduced by the static booster curves. Starting from this consideration, some authors developed a model of assistance based on the hydraulic behavior ([4], [5], [9]),
To adapt the standard assistance to patients with disabilities, it is possible to refer to the theory of the position control with gravity compensation, that is widely diffused in the robotics for regulation tasks of robot manipulators with elastic joints [16, 15, 19]. The same principle can be applied to provide the assistance in case of disabled drivers, under the hypothesis that it can help the driver on his driving accuracy and, in some cases, to reduce his driving effort. The compensation represents an additional torque, that modifies the standard assistance according to the cruise speed of the vehicle. At high speeds, the main goal is the tracking position: for instance, the weight compensation helps to perform a predefined path during an emergency manoeuvre or to maintain the equilibrium position on the steering wheel during cruise control. At low speeds, the compensation improve the driver's comfort. The muscular torque is an active load, that acts according to the direction of the movement. The torque due to the weight is a passive load, acting always in the same direction. According to the direction of the movement, it accelerates or brakes the muscular torque. For this reason, it needs to be compensated when he behaves as a brake, but it is useful to improve the driver's comfort in the opposite case. To join these requirements with the diffused technology the following assistance model is proposed:

$$\dot{\xi} = \begin{cases} -a\xi - b\sqrt{|\xi|}\dot{\hat{\theta}}_v + c(\sqrt{|\xi| + \varepsilon})\hat{\tau}_m, & \text{if } |\xi| \leq \xi_{max} \\ 0, & \text{else} \end{cases} \tag{25}$$

with the assistance torque τ_{ass} is given from

$$\tau_{ass} = \underbrace{(h_1(V) \times \xi)}_{Assistance} - \underbrace{\tau_w(\hat{\theta}_v) \times \left[(1 - h_1(V)) + \frac{h_1(V)}{2}(1 - \text{sign}(\hat{\tau}_m \times \tau_w(\hat{\theta}_v))\right]}_{Compensation} \tag{26}$$

where $\dot{\hat{\theta}}_v$ and $\hat{\tau}_m$ correspond, respectively, to the estimated steering rate and the estimated muscular torque, obtained from the observer developed in Section 3. The function $h_1(V)$ determines the transitions between the assistance provided at high speeds and the assistance at lows speeds of the vehicle V. The disturb $\tau_w(\theta_v)$ to be compensated is defined in Eq. (23). The output of the previous differential equation saturates, as soon as ξ reaches the maximum ξ_{max}, admitted from the electrical motor. The values to tune the assistance model allows to the module Gipsa-Tuning.

The assistance provided by this model in steady-state ($\dot{\xi} = \dot{\theta}_v = 0$) for two range of speed of the vehicle (V = 0 and 30 km/h) is shown in Figs. 6 and 7, for a driver's torque between $\pm 5Nm$ all over the steering plane.
The weight disturb is positive for all $\theta_v > 0$, while it is negative when $\theta_v < 0$. For V = 0 km/h, when the muscular torque $\tau_m > 0$ and we are in the negative plane of the disturb, then the compensation acts, otherwise it is not active (see Fig. 6). At V = 30 km/h, the compensation is always active, modifying everywhere the classical assistance (see Fig. 7).

5 NeCS-CAR TELEOPERATION SETUP

The proposed methodology can be validated experimentally on the dedicated platform NeCS-CAR funded by the *NeCS Team* at the Control System department of GIPSA-lab, shown in Fig. 8. A remote operator can drive the car via a hybrid (Ethernet + WLAN) networked communication by observing the video and experiencing the torque feedback. A PC-unit is installed on the control station. The embedded network is switched Ethernet to communicate between the controller, the image processor and IP video camera. These devices are connected with a 100 Mps switch that is further connected to a WLAN router.

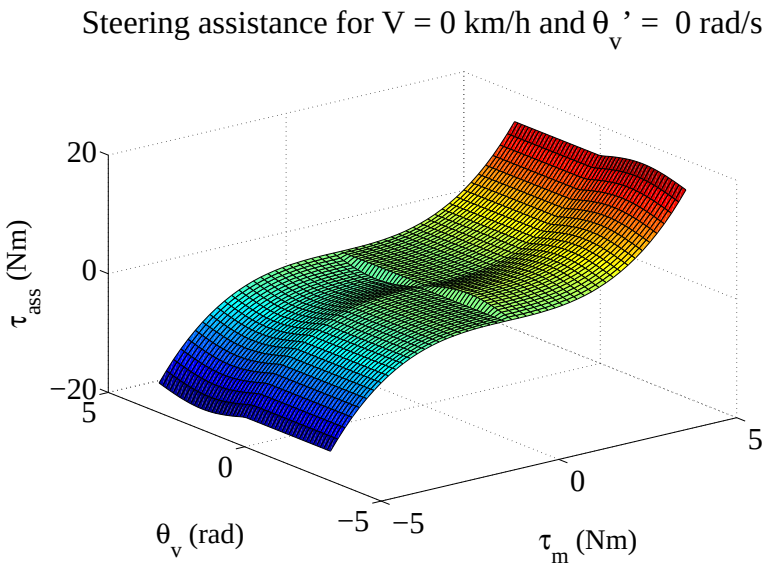

Figure 6: Behavior of the assistance system at 0 km/h

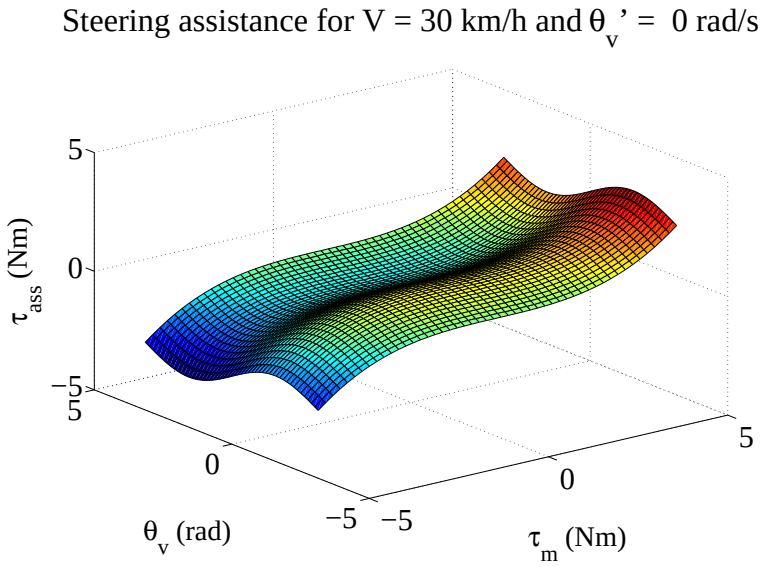

Figure 7: Behavior of the assistance system at 30 km/h

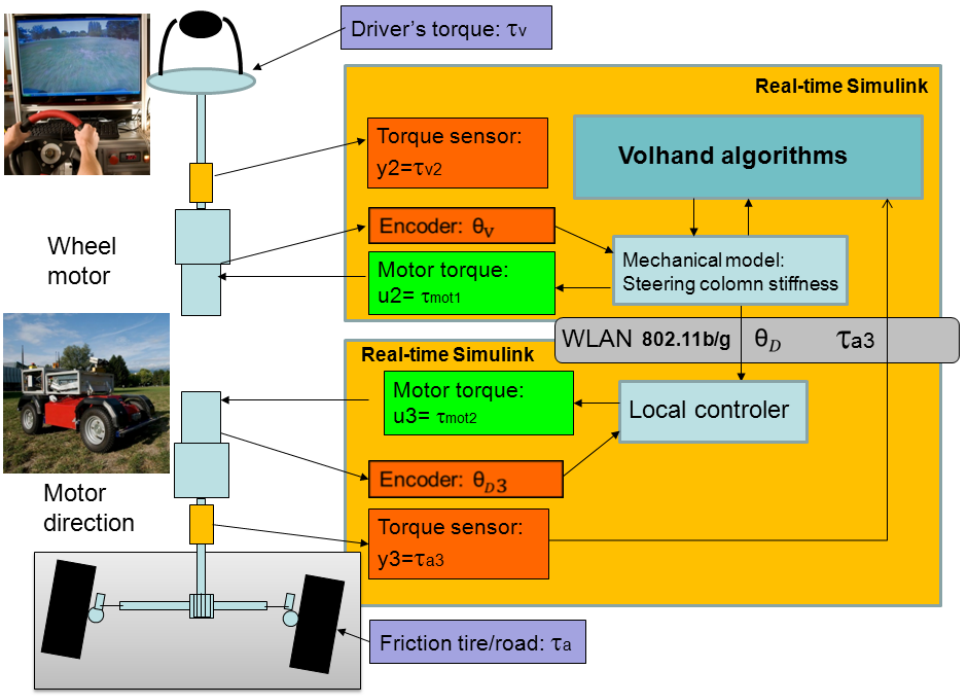

Figure 8: NeCS-CAR teleoperation setup (NeCS Team GIPSA-lab/INRIA)

5.1 Control station

The operator can drive on a steering wheel with its motor-shaft column. At the basis of the steering column, there are a torque and a force sensor. For the current study, the only torque sensor is considered. It sends the measured driver's torque to the PC-unit (signal $y_2 = \tau_{v2}$ in Fig. 8). A brushless motor takes in input the reference torque from the PC-unit (signal $u_2 = \tau_{mot1}$ in Fig. 8) and gives into output the measure of the steering wheel position θ_v.

5.2 PC-unit

The operating system on the PC-unit is Windows XP®. For real time communication of the controller, Ardence RTX interface is used. Controller is designed in Matlab 2007® and it is converted to Real Time Execution (RTX), that is a rapid prototyping product by Quanser. Real time TCP/IP, included with RTX, provides tools to embed high performance real-time networking protocols into systems and applications. This is possible with the A/D and D/A converters on the Data Acquisition and Control Buffer (DACB) communicating with WinCon using the RTX Workshop installed in Simulink.
The PC-unit sends the torque feedback to the control station. The torque feedback is the sum of simulated and measured elements. Among the simulated ones, it is possible to find the control input u to compensate the oscillations of the steering wheel. The torsional torque $k(\theta_v - \theta_s)$ is also simulated to obtain the value of motor-shaft angle θ_s. The driver's assistance systems are also simulated. Concerning the tire-road friction torque, it can be obtained by simulation or throughout the use of the NeCS-CAR. In simulation, the LuGre friction model, shown in Section 2.3 is implemented in Simulink.

5.3 NeCS-CAR

When the NeCS-CAR is linked to the pc unit, it receives the input control from the steering wheel via teleoperation; this input allows it to move their wheels according to the position θ_s at the desired cruise speed. A torque sensor mounted on the direction column of the NeCS-CAR allows to measure the real friction torque, that is used to replace the LuGre model in the HIL setup.

6 VALIDATION OF THE GENERAL ARCHITECTURE

This section describes the experimental validation of the proposed general architecture. The first part introduces the steps to adapt the state-space model to the hardware configuration. The second part consists into the validation of the oscillation annealing control and of the torque observer. This LuGre tire-road friction model is also validated experimentally with a comparison with the measured friction torque obtained from the NECS-CAR. Finally, the adaptation methodology is also tested in simulation and on the hardware setup for some scenarios of interest.

6.1 Adaptation of the state-space model to the HIL setup

In Eq. (1), authors consider an initial value for the steering wheel inertia J_v and viscosity B_v, that may not completely correspond to the real value of the system. For this reason, let make the following assumption:

Assumption 1: let define J and B the difference between the values adopted in simulation (respectively, J_v and B_v) and values of the setup system (respectively, J_0 and B_0), that have to be identified :

$$J = J_v - J_0 \tag{27}$$
$$B = B_v - B_0 \tag{28}$$

Let substitute J_v and B_v, as resulting from Eqs. (27) and (28), in Eq. (1), as follows:

$$(J_0 - J)\ddot{\theta}_v + (B_0 - B)\dot{\theta}_v = \tau_v - k(\theta_v - \theta_s) \tag{29}$$

and let apply the Laplace transform to obtain the value of θ_v, as function of the driver's torque τ_v and the total torque C_m, as follows

$$(J_0 - J)s^2\theta_v + (B_0 - B)s\theta_v = \tau_v - k(\theta_v - \theta_s) \tag{30}$$

Let divide the real inertia and viscosity from the residual ones:

$$(J_0 s^2 + B_0 s)\theta_v = \tau_v - k(\theta_v - \theta_s) + (Js^2 + Bs)\theta_v \tag{31}$$

it follows that

$$C_m = -k(\theta_v - \theta_s) + (Js^2 + Bs)\theta_v \tag{32}$$

is the simulated torque given to the motor and

$$\theta_v = \frac{1}{(J_0 s^2 + B_0 s)}(\tau_v + C_m) \tag{33}$$

is the real steering wheel angle, obtained from the steering wheel and the column.
Let apply the same procedure in Eq. (2) to obtain the relation between the steering wheel position θ_v and the column-shaft angle θ_s. The Laplace transform produces:

$$J_T s^2\theta_s + N_2^2 B_m s\theta_s = k(\theta_v - \theta_s) + \frac{\tau_a}{N_1} + N_2 u \tag{34}$$

By collecting all the terms in θ_s, it is possible to obtain:

$$\theta_s = \frac{1}{J_T s^2 + N_2^2 B_m s}\left(k(\theta_v - \theta_s) + \frac{\tau_a}{N_1} + N_2 u\right) \tag{35}$$

Eqs. (33) and (35) are sufficient to adapt the state-space representation to the HIL model. Preliminary simulations showed that the two models are equivalent.

6.2 Parameter identification

The values J_0 and B_0 are obtained with the following procedure:

1) we apply on the open loop system a Pseudo-Random Binary Sequence (PRBS) input sequence of C_m, output of the pc-unit.

2) We collect the measured values of the motor angular speed θ_m and we make the hypothesis that the model behaves as a first order transfer function of the form:

$$G_0(s) = \frac{\dot{\theta}_v}{C_m} = \frac{k}{1 + T_p s} = \frac{1}{B_0 + J_0 s} \tag{36}$$

Under this hypothesis, the parameters to identify correspond to:

$$J_0 = \frac{T_p}{k} \tag{37}$$

$$B_0 = \frac{1}{k} \tag{38}$$

The solution of this problem is obtained by applying a non-linear least squares algorithm, implemented with the software Matlab 2011®. The resulting values are Table 1.

6.3 Experimental validation of the oscillation annealing control (Gipsa-Comp)

6.3.1 Steering column in open loop

Previous studies [11] showed that the system becomes unstable, when there is a variation of the driver's exerted torque. The instability is physically due to the torsion of the steering column. From a mathematical point of view, it can be checked with the two imaginary poles of the state matrix of the system ($p_{1,2} = -1.0023 \pm 56.0151i$), while the last pole is stable ($p_3 = -4.9386$).
To test the effect of this instability, in [11] authors applied a constant torque for a certain time and then they left the steering wheel. The simulations of the system showed important oscillation on the steering wheel rate . To verify this behaviour on the HIL setup, authors applied the input trajectory shown in Fig. 9(a): the operator turns the steering wheel in clockwise of 90 °, then leaves it for 4 s and repeats the manoeuvre in anti-clockwise. Fig. 9(a) shows the response of the real system in terms of angular speed of the steering wheel: when the driver leaves the system, the steering system starts to oscillate (it is evident at times between 4 and 6 s). It stops when all the energy of the system is dissipated. This experimental results is compatible with the simulations, shown in [11]. Nevertheless, it is possible to make a further check by applying the same input trajectory also on the simulated system. The PID controller acts as the human operator, taking in input the real reference trajectory and applying the corresponding exerted torque. In Fig. 9(a) it is possible to verify the presence of the oscillations on the steering column: note that their amplitude corresponds to the real amplitude that we measure on the experimental setup. As stated in [11], these oscillations are uncomfortable for the driver and moreover they affects the measure of the torsion, that is commonly used to measure the driver's torque to give in input to the booster stage. For these reason, it is necessary to compensate them with a proper controller.

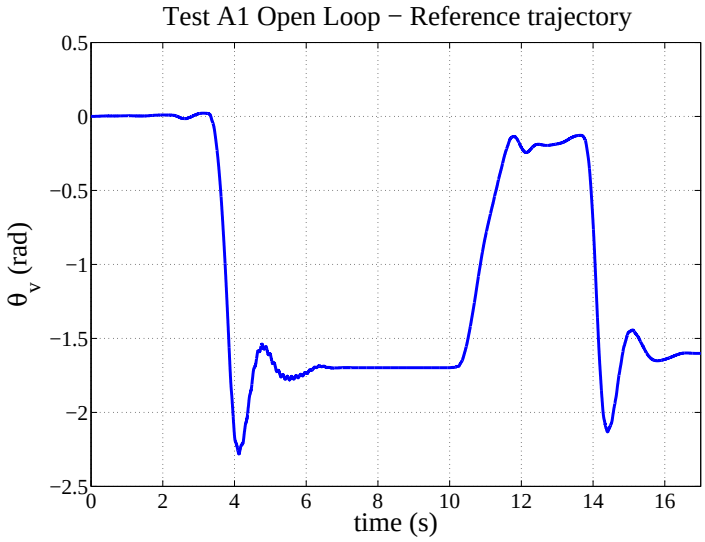

(a)

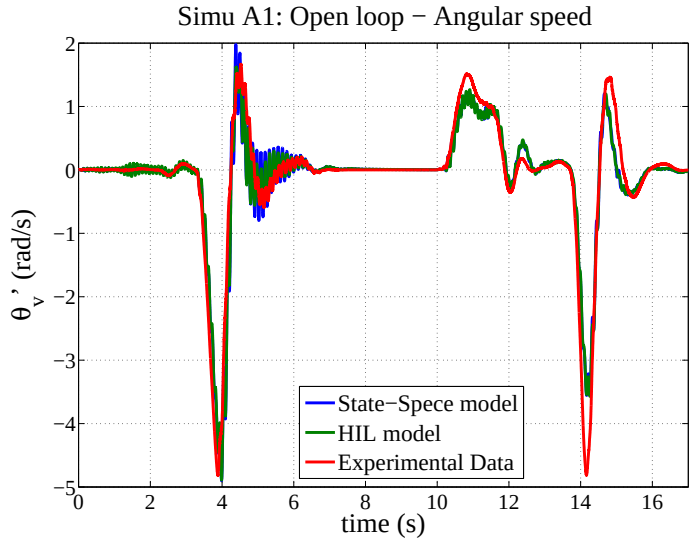

(b)

Figure 9: (a) Steering wheel trajectory applied from the operator on the system. (b) Response of the EPS system in terms of steering wheel rate. Note the oscillations of the systems between 5 and 8 s.

6.3.2 Steering column in closed loop

The oscillations shown in previous section can be annealed by introducing an optimal LQR control, under the constraint to not alternate the impedance between the driver's and the load torque at low frequency. The theory concerning the synthesis of this controller is shown in [11].
The exerted driver's trajectory is shown in Fig. 10(a) and is similar to the open loop case: it corresponds to turn the steering wheel from the initial position to 100 ° in anticlockwise, then releasing the wheel for 6 s and finally making another turn in clockwise.
Fig. 10(b) shows the angular speed of the steering wheel: despite the open loop case, the oscillations are completely annealed by the effect of the inner control. This result validates the simulations, shown in [11], where the input to the system is the driver's exerted torque.
To validate the PID controller used to simulate the driver's behavior, authors took the experimental data concerning the steering wheel trajectory and put them as reference input in the simulated models (state-space representation and the model based on the transfer functions). Fig. 11(a) shows that the steering wheel trajectories for the two models follow the experimental trajectory, while Fig. 11(b) shows also a comparison between the column torsion measured during the experiment and the simulated one. This measure is not affected any more from the oscillations of the steering wheel and provides a more correct estimation of the driver's exerted torque. These results show that the PID controller attempts to its design objectives: to make a position tracking and to provide a realistic torque for the system, in order to obtain a realistic behavior of the simulated system.

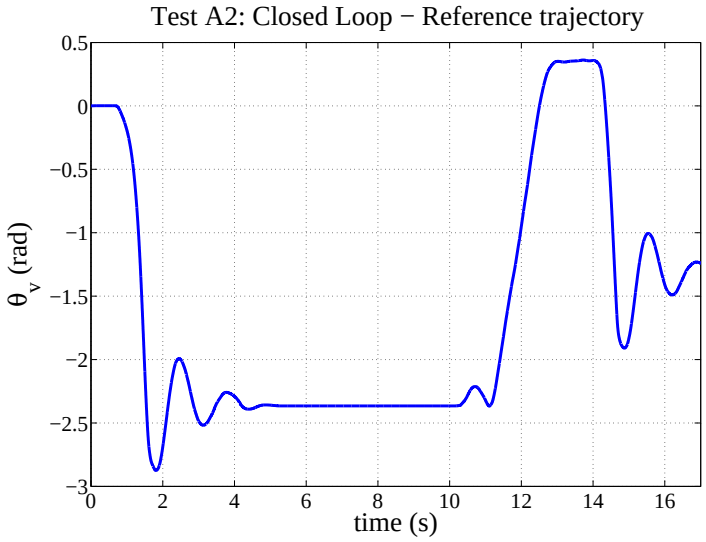

(a)

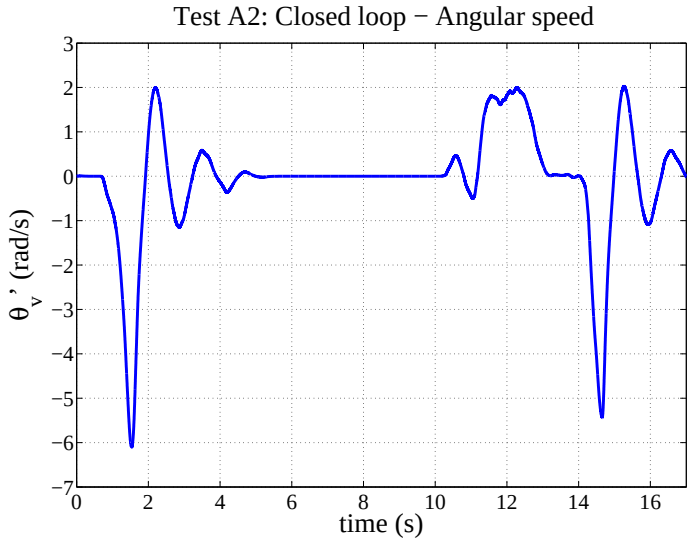

(b)

Figure 10: Angular position (a) and angular speed (b) of the steering wheel. The oscillations of the steering column are annealed by the LQR control.

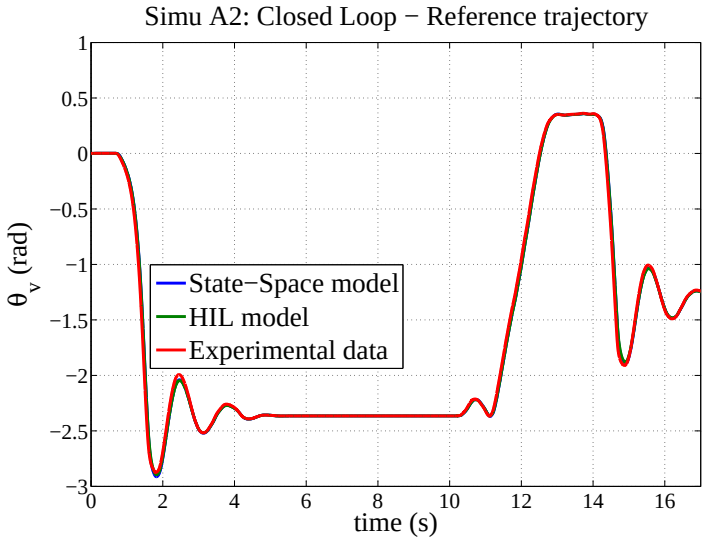

(a)

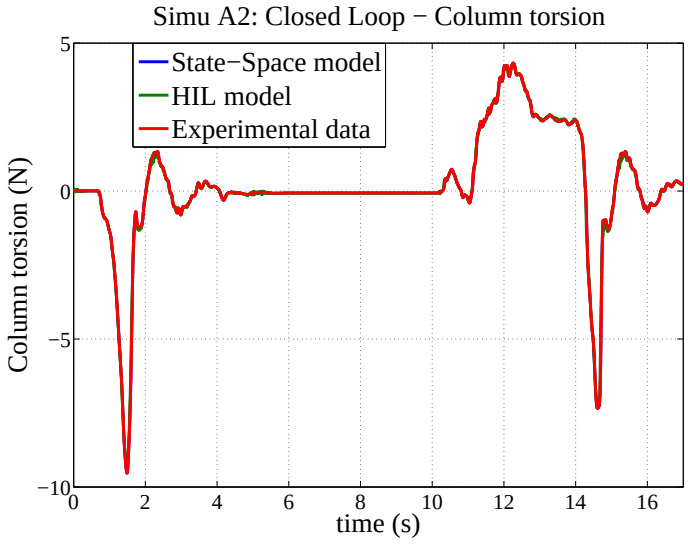

(b)

Figure 11: The simulation (on the left) and the experimental validation (on the right) of the oscillation annealing control.

6.4 Experimental validation of the observer performance (Sect:GipsaObs)

6.4.1 Validation of the driver's torque estimation

In [11], the observer was designed by using the measures of the steering column rate $\dot{\theta}_s$ and of the torsion $k(\theta_v - \theta_s)$. To validate the performances of the observer, let consider the case of a trajectory exerted by a driver, who can manoeuvre with two hands, with the oscillation annealing control to prevent oscillations of the steering column, but without the support of the assistance. The applied trajectory on the steering wheel is shown in Fig. 12(a), while the comparison between the estimated torque $\hat{\tau}_v$ and the measured one C_{mmeas} is shown in Fig. 12(b). The numerical noise (affecting $\dot{\theta}_s$) and the measure noise (affecting the torsion) do not modify the observer performance. They increase when the angular speed and acceleration of the steering column augment. This is due to the influence of the mechanical parameters on the model. For this reason, in Fig. 12(b) it is also shown the profile of the angular speed of the electrical motor.

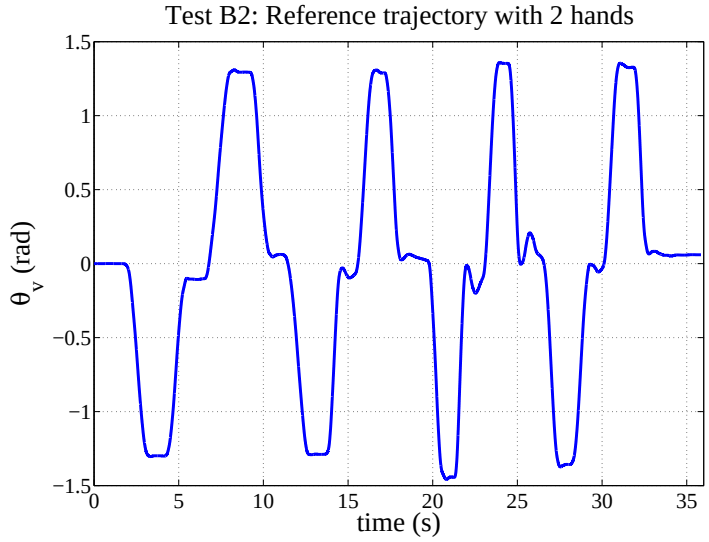

(a)

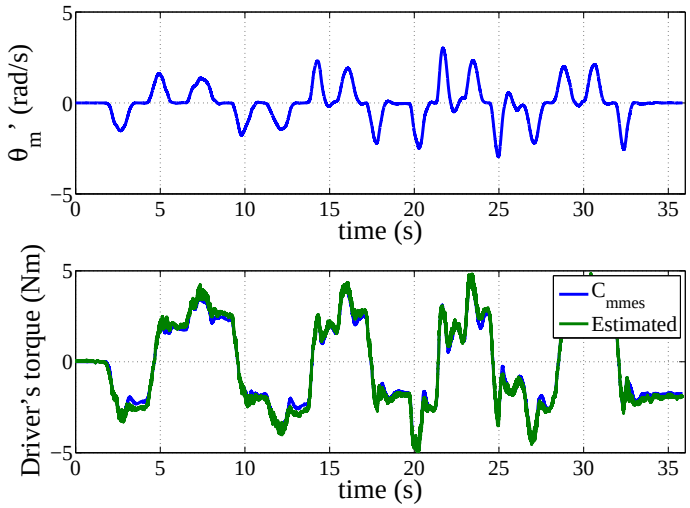

(b)

Figure 12: Observer validation: (a) Trajectory imposed on the test, with two hands and oscillation annealing control. (b) Profile of the angular speed of the electrical motor and comparison of the estimated torque with the driver's torque measure C_{mmeas}

6.4.2 Validation of the tire-road contact friction estimation at stand-still

The comparison between the estimated torque $\hat{\tau}_a$ and the output of the LuGre sticking torque allows to validate the observer performance in this case, as shown in Fig. 13. The estimation error is negligible and the observer performance are satisfying. It is also possible to note that if we divide this value assumed by the torque at low frequency (about 30 N m) by the gear ratio $N_1 = 13.67$, we obtain the value of the driver's torque during the same instant (about 2.2 N m), meaning that the LQR control preserve the impedance relation between the two torques. This is property cannot be verified at high frequency, because of the influence of the angular speed and acceleration of the steering wheel.

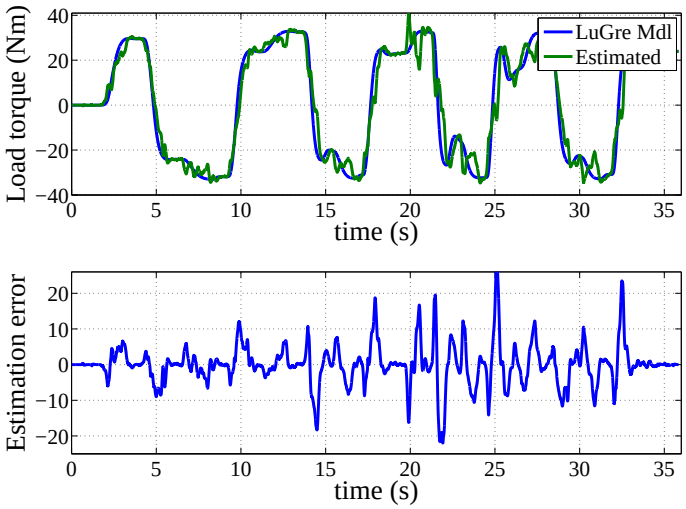

Figure 13: From the top to the bottom: comparison of the estimated torque with the load torque, obtained from the LuGre model, and estimation error.

6.4.3 Comparison with the real friction torque at stand-still

A further validation of this tire-road friction model can be done, using the torque measures obtained with the NeCS-CAR. Moreover, the performance of the observer can be tested to verify that it is able to retrieve the real friction torque profile.
In Fig. 14(a), the comparison between the simulated friction torque and the real measures obtained from the NeCS-CAR is proposed. It is possible to observe that the simulated torque is realistic, if compared to the measured one. Nevertheless, to improve the model a parameter tuning or identification can be done. In Fig. 14(b), the estimated torque is compared with the measured one. In spite of the measurement error, the observer performances are globally satisfying. It is possible to diminish the transient error at the cost of a high gain of the observer.

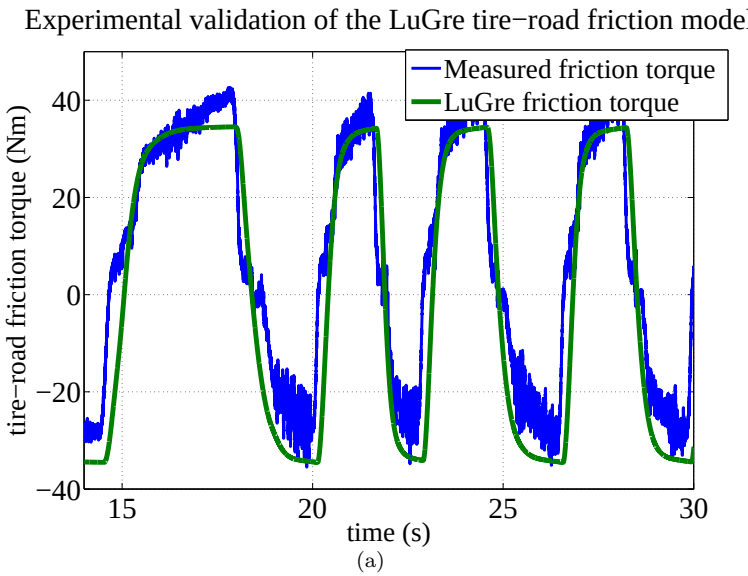

(a)

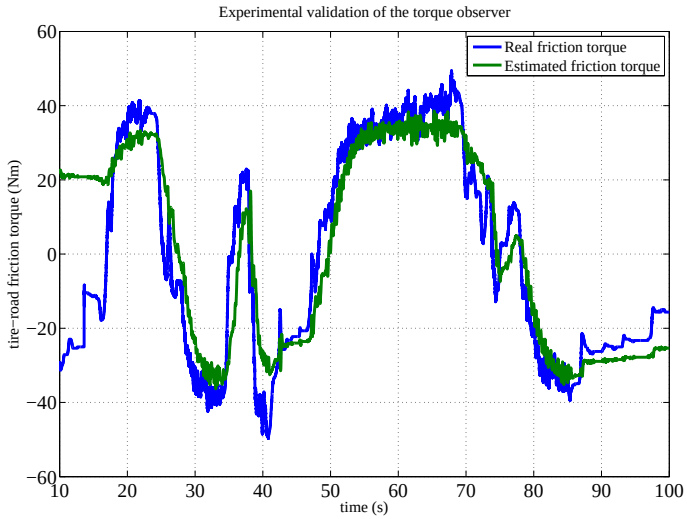

(b)

Figure 14: (a) Comparison between the measured friction torque and the simulated one (b) Observer performance into the estimation of the friction torque sensed from the NeCS-CAR.

6.4.4 Validation of the tire-road contact friction in movement (Self-Alignment torque)

The following additional test has been done to validate the model used to describe the Self-Alignment torque. In [11], authors showed that this torque appears as the vehicle speed grows up and tends to rotate the wheels around its vertical axis in order to make them return to the straight position. The Self-Alignment model adopted in [11] needs as input the measure of the slip angle, that is a measure at the origin of the lateral forces acting on the vehicle during turning manoeuvres. To obtain this value, in [11] authors used an approximated relation between the vehicle speed v and the radius of curvature ρ, given by the curve traced by the vehicle in a given moment, i.e. $\beta(t) = f(v, \rho)$. To improve this results, in this case, authors use the common form of the linear bicycle model.

6.4.5 Dependency of the simulated models from the speed of the vehicle

In [11], authors validated the friction torque by verifying that the simulated results follow the expected logic, according to the variations of the speed of the vehicle. At this aim, several simulations were carried out for velocities going from 0 to 30 $\mathrm{km\,h^{-1}}$ and over a range time of several seconds, in order to see the effects at steady-state. The choice of this speed range is due to the fact that an EPSs operate in this range. The same tests have been carried out also on the HIL setup: in this case, we look at the input steering wheel angle, corresponding at 30 °. The steering ratio N_1 induces an angle of curvature of the wheels of about 2 °. This results is consistent with the actual technologies, where the steering ratio is 15 for power assisted vehicles and 18 for non-assisted ones. The steering angles and the corresponding angles at the wheels of the vehicle are shown in Figs. 15(a) and 15(b) for the range of speeds of interest. The corresponding wheel torques are shown in Figs. 16(a) and 16(b). These results validate what it has been shown in [11]. Note that, even if the two friction models are simulated, they differs in terms of input signals, that are simulated in [11], while they correspond to real measure in the HIL setup. They differ also because of the slip angle. The effect to have the same behaviour helps to validate the numerical approximation, used in [11]. Next step in this sense is to verify this behaviour with the *NecsCar*, in order to obtain a real friction torque and validate the performance of the observer in this case.

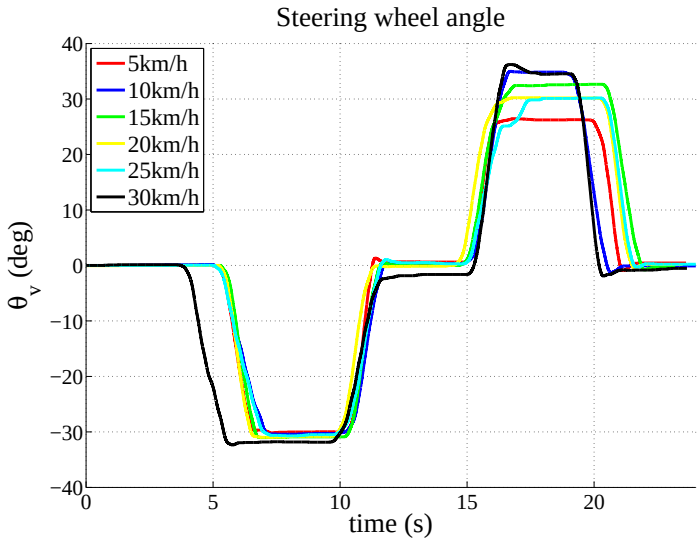

(a)

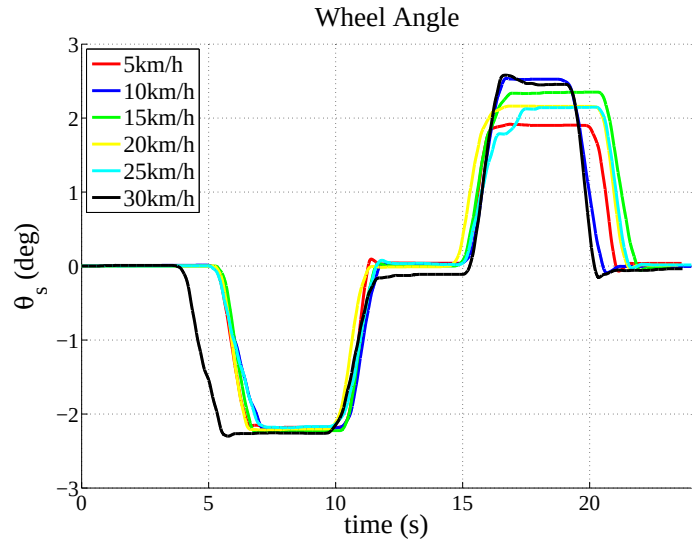

(b)

Figure 15: (a) Steering wheel trajectory and (b) corresponding angle of wheels of the vehicle.

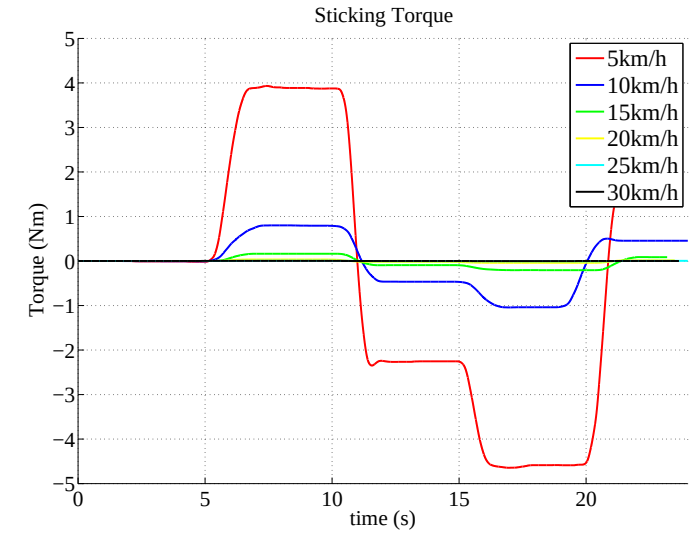

(a)

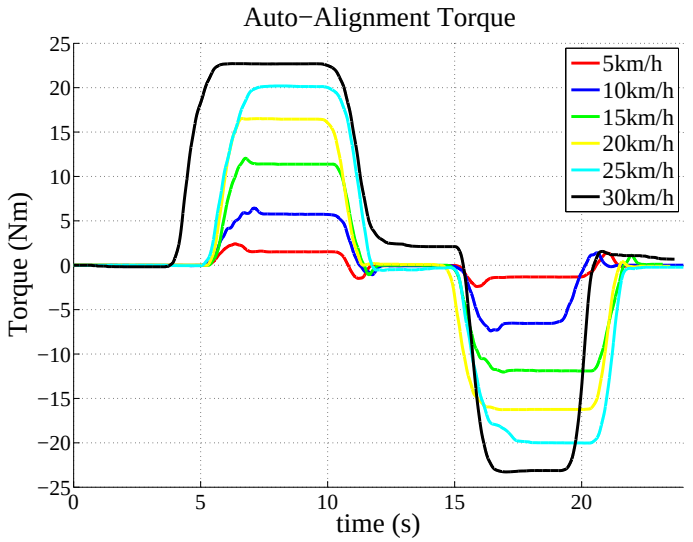

(b)

Figure 16: (a) Sticking and (b) Self-Alignment torque for different speeds of the vehicle.

6.5 Scenario for the validation of the driver's assistance system (Gipsa-Booster)

To test the proposed methodology, three scenarios are considered. For each scenario, the simulations results are compared with the corresponding experimental tests and two performance metrics are introduced: the driving precision and the driving strain/comfort.
The driving precision is defined as the error e between the reference trajectory and the current value of the steering wheel angle:

$$D_p = \int_0^T (\theta_{ref} - \theta_v)^2 dt \tag{39}$$

and the objective of the assistance is to minimize this error.
A preliminary metrics to validate the assistance into the improvement of the driver's strain is the driver's energy E_d exerted during the driving task. It is considered into absolute value, because driver's muscles are not reversible. The definition of this metrics is the following:

$$E_d = \int_0^T |\tau_m(t) \times \dot{\theta}_v| \mathrm{d}t \tag{40}$$

Moreover, the effort to maintain the same position over a long time can be shown only with the use of electromyography (EMG), that may reveal the contraction and co-contraction faction of the muscles involved during the driving. An alternative criteria, that can be employed is the driver's Strength, defined as follows:

$$S_d = \int_0^T |\tau_m(t)|^2 \mathrm{d}t \tag{41}$$

For each study case, the corresponding improvement criteria is shown in Table 3.

Scenario	Vehicle speed	Ball position	Metrics
Parking manoeuvre	0 km/h	0° / 90°	Driver's energy E_d
Obstacle avoidance	30 km/h	0° / 60°	Driving precision D_p
Cruise control	30 km/h	0° / 60°	Driver's Strength S_d

Table 3: Summarizing table with simulation/test scenarios and corresponding improvement critera

Each scenario is simulated (and tested) under 3 different models of the driver, in order to verify the effects of the proposed assistance.
The first test corresponds to the ideal case without the disturbance of the arm. The tracking controller takes in input the error between the reference trajectory and the current path and exerts the corresponding delayed torque on the steering wheel $\tau_v = \tau_m$. The second simulation corresponds to the case where the weight of the arm acts as a disturb on the tracking controller $\tau_v = \tau_m + \tau_w$, but the steering assistance is not activated. Finally, the last simulation corresponds to the same as in the second case, but the steering assistance is active $\tau_v = \tau_m + \tau_w - U_g$.
For sake of simplicity, the experimental validation has been done considering only the driving models of the second and the third simulations. For each scenario, the first test is done with the operator who drives with one hand, but without the steering assistance. The second test is done with the operator who drives with one hand and the assistance active.
In all cases (simulations and tests), the LQR control is active, the observer provides the estimated muscular torque to the steering assistance and the friction torque is simulated. Further tests are in progress to validate the methodology with the NeCS-CAR.

6.5.1 Parking manoeuvre

A ramp is given in input to the PID controller as reference trajectory for a speed of the vehicle at 0 $\mathrm{km\,h^{-1}}$ for the different models of the driver. Under these conditions, the main responsible of the road feeling feedback is the Sticking torque. This is the case, when the steering assistance system acts to diminish the driver's effort and it is active only when the driver's movement is in the opposite sense of the weight force.
Let consider the case with the position of the ball on steering wheel is at 0°. In Fig. 17(a) the reference trajectory is compared with the resulting trajectory at the output of each driver's model. It is evident the influence of the disturbance on the second model, when he tries to gain the straight position (at

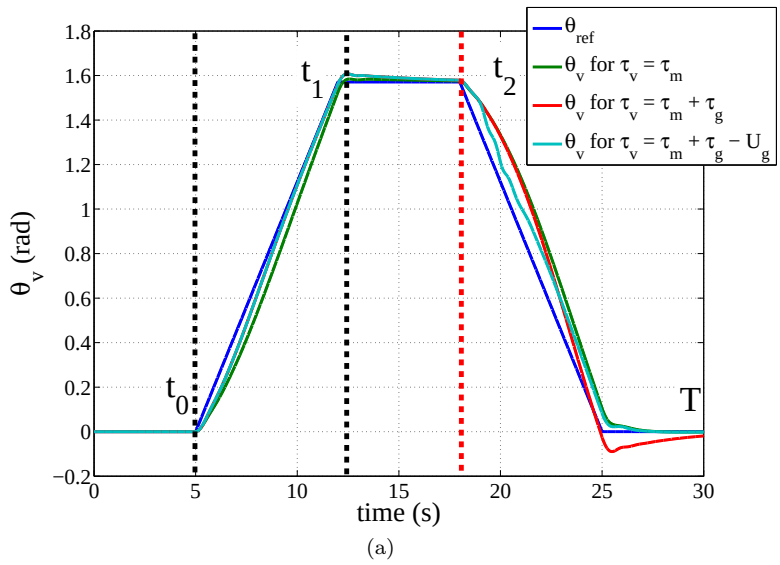

(a)

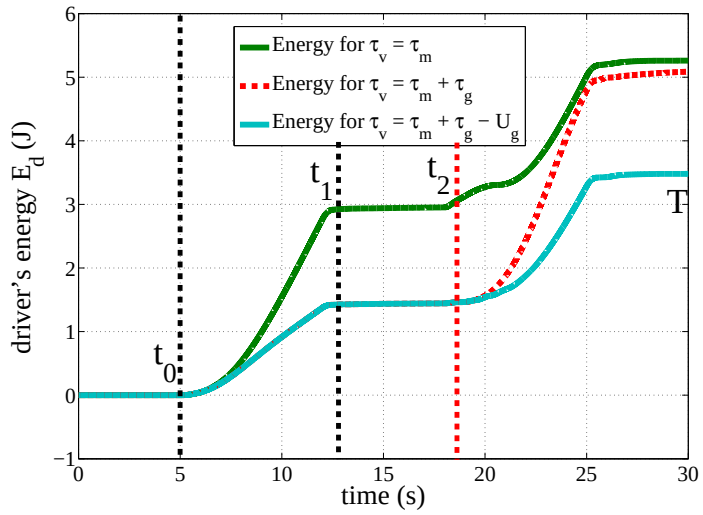

(b)

Figure 17: (a) Profile of the trajectory of the steering wheel used to simulate parking manoeuvre. (b) Profile of the mechanical power dissipated during the simulation.

25 s), while this disturbance is annealed by the steering assistance acting on the third model. In this scenario, it is possible to observe how the assistance helps to reduce the driver's strain (see Fig. 17(b)): during the first part of the simulation (at 10 s), the assistance is not active, because the weight helps the driver's movement, so the curve of driver's strain overlaps the curve corresponding to the second model, without assistance. During the second part, the compensation is active and the curve of strain overlaps that one corresponding to the first model, with a global improvement of the driving comfort. The experimental test concerning this scenario is shown in Fig. 18(a). To be able to compare the two experiences, a constraint in terms of timing and speed of the movement has been required to the operator. A fast movement entails the growth of the angular speed of the steering wheel, with a consequences on the measure of the mechanical power. Experimental results shown in Figs. 18(a) and 18(b) validate the simulation results. The real movement is comparable with the simulated one and it is possible to verify the diminishing of the mechanical power. For both the situations, it is possible to show the drive's power consumption over the steering wheel plane (see Figs. 19 and 20). In both figures, the power consumption is shown during 2 parts of the movement: from 0° to 90° the movement is in the same direction as the weight disturb, so the assistance does not compensate. When the movement is in the opposite sense despite the disturb, the assistance helps to diminish the driving power. It is possible to remark that the magnitude of the power in test is compatible with that one obtained in simulation.

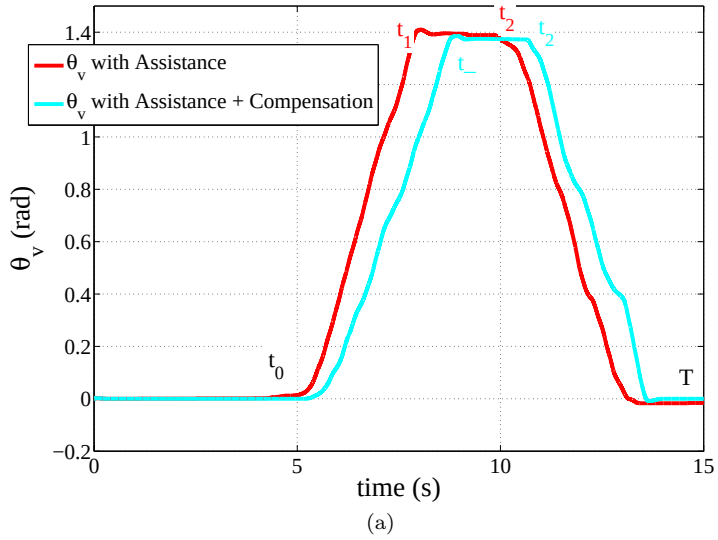

(a)

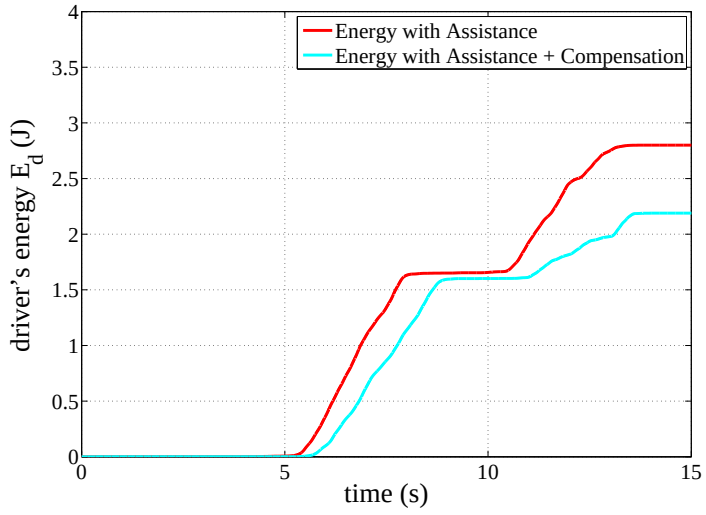

(b)

Figure 18: (a) Profile of the trajectory of the steering wheel used to test the parking manoeuvre on the HIL setup. (b) Profile of the mechanical power dissipated during the test.

6.5.2 Obstacle avoidance

To simulate the scenario of an obstacle avoidance, a step-wise reference trajectory is given in input to the tracking control. The vehicle is simulated with a cruise speed of 30 $\mathrm{km\,h^{-1}}$, meaning that the Self-Alignment torque is the main responsible of the driver's steering feel. The driver's steering assistance is always active to compensate the disturbance and to improve the driving precision. The simulations results are shown in Fig. 21(a) with the 3 different driver's models.The influence of the disturb on the tracking control is clear, when it tries to change path direction, for instance, at the 5 second. On the experimental validation, this phenomenon is not evident, so as it happens in simulation. The requirement to reproduce exactly the same movement over a long period introduce many difficulties on the experiment and the behavior of the driver is probably different with respect to the model used in simulation. Anyway, it is possible to find some cases where the improvement is evident, as it is shown in Fig. 21(b).

6.5.3 Cruise control

The effect to maintain the same straight position for a long time may infer with driver's strain. In this case, the steering assistance helps to maintain the path following at high speeds and to improve the driving comfort. It is possible to verify and test the diminishing of the driver's strain to maintain for

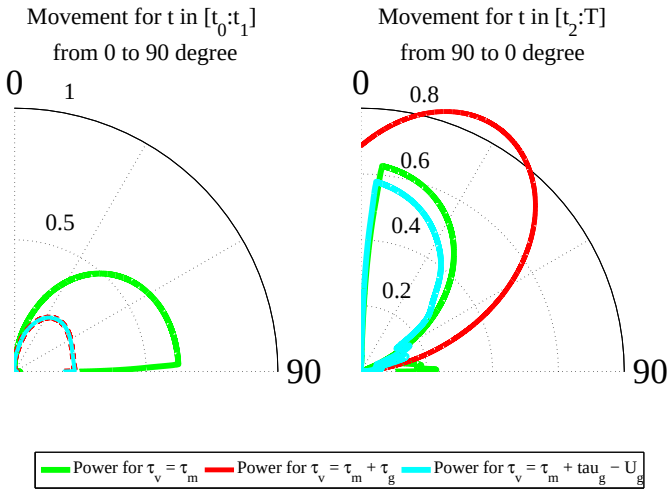

Figure 19: Power consumption during the simulation

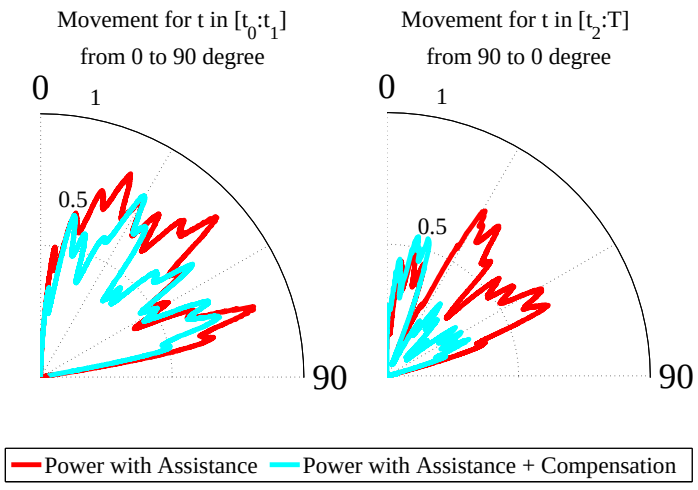

Figure 20: Power consumption during the experimental test

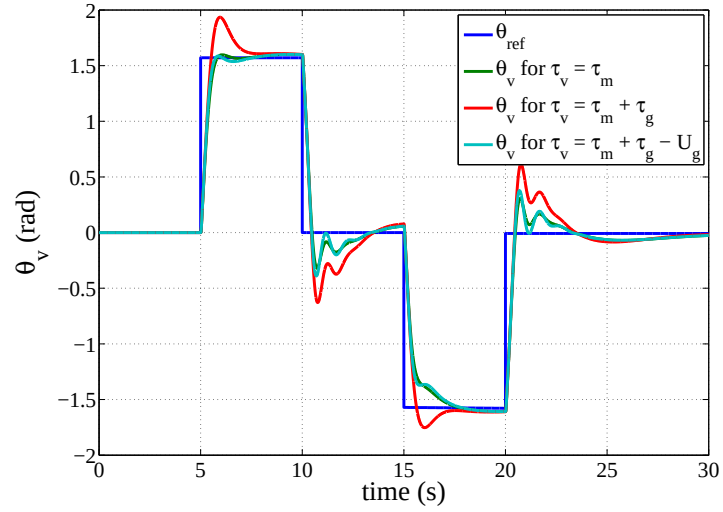

(a)

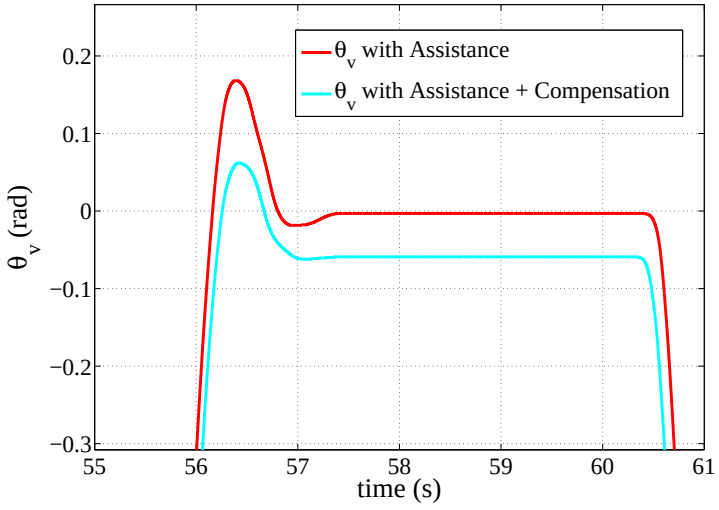

(b)

Figure 21: (a) Profile of the trajectory of the steering wheel used to simulate obstacle avoidance. (b) Zoom of the profile of the trajectory applied on the HIL setup, where the contribution of the steering assistance is evident.

long time the same position.

7 Conclusions

A methodology of adaption of generic steering assistance laws was developed and validated experimentally. This methodology can be used in case of a driving with 1 or 2 arms. The improvements due to this methodology can be shown in Table 7. It is not exhaustive, because it is not possible to obtain the percentage of improvements for all the cases, but it provides a preliminary idea. For the parking, all criteria are improved in simulation and tests. The obstacle avoidance cannot be verified in test, yet. The cruise control always find an improvement from the introduction of the assistance, because it is active all the time. On the other hand, the muscular contraction and co-contraction to maintain the same position over a long time (cruise control scenario) can be shown only with the electromyography (EMG). Further EMG tests are planned to validate this metrics.
The driver's model can be improved to keep into account more pathologies, that can deal with the project VolHand. Finally, the study concerning the asymmetry abilities of the driver is under development.

	% improvement		
	Energy	**Strength**	**Precision**
Parking	31.5 simu 23 test	16.9 simu 23.04 test	76.4 simu n.a.
Obstacle avoidance	n.a. simu	n.a. simu	24.4 simu
Cruise control	n.a.	100	n.a.

References

[1] Jrgen Ackermann and Deutsche Forschungsanstalt. Yaw disturbance attenuation by robust decoupling of car steering. *Control Engineering Practice*, 5:1131–1136, 1996.

[2] A.W. Burton. Innovation drivers for electric power-assisted steering. *Control Systems, IEEE*, 23(6):30–39, Dec. 2003.

[3] Poussot-Vassal C. *Commande robuste lpv multivariable de chassis automobile*. PhD thesis, Grenoble Institut Polytechnique, 2008.

[4] C. Canudas de Wit. Fun-to-drive by feedback. In *Decision and Control, 2005 and 2005 European Control Conference. CDC-ECC '05. 44th IEEE Conference on*, page 13, dec. 2005.

[5] C. Canudas de Wit, X. Claeys, and H. Bechart. Stability analysis via passivity of the lateral actuator dynamics of a heavy vehicle. In *Control Applications, 1999. Proceedings of the 1999 IEEE International Conference on*, volume 2, pages 1371–1376, 1999.

[6] C. Canudas de Wit, S. Guegan, and A. Richard. Control design for an electro power steering system: Part i the reference model. *European Control Conference*, Sept. 2001.

[7] C. Canudas de Wit, T. Panagiotis, E. Velenis, M. Basset, and G. Gissinger. Dynamic friction models for road/tire longitudinal interaction, 2002.

[8] R.C. Chabaan. Optimal control and gain scheduling of electrical power steering systems. In *Vehicle Power and Propulsion Conference, 2009. VPPC '09. IEEE*, pages 53–59, Sept. 2009.

[9] X. Claeys, C. Canudas de Wit, and H. Bechart. Modeling and control of steering actuator for heavy duty vehicle. In *European Control Conference*, 1999.

[10] R.A. Hess and A. Modjtahedzadeh. A control theoretic model of driver steering behavior. *Control Systems Magazine, IEEE*, 10(5):3 –8, aug. 1990.

[11] J.T. Illán, V. Ciarla, and C. Canudas de Wit. Oscillation annealing and driver/tire load torque estimation in electric power steering systems. In *Control Applications (CCA), 2011 IEEE International Conference on*, pages 1100–1105, Sept. 2011.

[12] K. Ji Hoon and S. Jae Bok. Control logic for an electric power steering system using assist motor. *Mechatronics*, 12(3):447–459, 2002.

[13] H. B. Jiang, J. B. Zhao, H. M. Liu, and L. Chen. Low-pass filter based automotive eps controller and comparative full-vehicle tests. In *Control and Decision Conference, 2008. CCDC 2008. Chinese*, pages 4662–4665, July 2008.

[14] W. Jiang, C. Canudas-de Wit, O. Sename, and J. Dumon. A new mathematical model for car drivers with spatial preview. In *18th IFAC World Congress*, 2011.

[15] Alessandro De Luca, Bruno Siciliano, and Loredana Zollo. Pd control with on-line gravity compensation for robots with elastic joints: Theory and experiments. *Automatica*, 41(10):1809 – 1819, 2005.

[16] R.C. Luo, C.Y. Yi, and Y.W. Perng. Gravity compensation and compliance based force control for auxiliarily easiness in manipulating robot arm. In *Control Conference (ASCC), 2011 8th Asian*, pages 1193 –1198, may 2011.

[17] S. Mammar and D. Koenig. Vehicle handling improvement by active steering. *Vehicle system dynamics*, 2002.

[18] H. Tsung Hsien, Y. Chih Jung, H. Shih Rung, H. Tsung Hua, and L. Ming Chih. Design of control logic and compensation strategy for electric power steering systems. In *Vehicle Power and Propulsion Conference, 2008. VPPC '08. IEEE*, pages 1–6, Sept. 2008.

[19] N. Ulrich and V. Kumar. Passive mechanical gravity compensation for robot manipulators. In *Robotics and Automation, 1991. Proceedings., 1991 IEEE International Conference on*, pages 1536 –1541 vol.2, apr 1991.

[20] E. Velenis, P. Tsiotras, C. Canudas De Wit, and M. Sorine. Dynamic Tire Friction Models for Combined Longitudinal and Lateral Vehicle Motion. *Vehicle System Dynamics*, 43(1):3–29, 2005.

[21] D.A. Winter. *Biomechanics and Motor Control of Human Movement*. Wiley, 2009.

[22] H. Zhang, Y. Zhang, J. Liu, J. Ren, and Y. Gao. Modeling and characteristic curves of electric power steering system. In *Power Electronics and Drive Systems, 2009. PEDS 2009. International Conference on*, pages 1390–1393, Nov. 2009.